AIRCRAFT FUEL TANK ENTRY WALL-PROJECTILE INTERACTION STUDIES

Kenneth Scott Bates, Jr.

Naval Postgraduate School
Monterey, California

June 1973

NAVAL POSTGRADUATE SCHOOL
Monterey, California

THESIS

AIRCRAFT FUEL TANK ENTRY WALL-PROJECTILE INTERACTION STUDIES

by

Kenneth Scott Bates, Jr.

Thesis Advisor: H. L. Power, Jr.

June 1973

54

UNCLASSIFIED

Security Classification

DOCUMENT CONTROL DATA - R & D

(Security classification of title, body of abstract and indexing annotation must be entered when the overall report is classified)

1. ORIGINATING ACTIVITY (Corporate author)

Naval Postgraduate School
Monterey, California 93940

2a. REPORT SECURITY CLASSIFICATION

Unclassified

2b. GROUP

3. REPORT TITLE

Aircraft Fuel Tank Entry Wall-Projectile Interaction Studies

4. DESCRIPTIVE NOTES (Type of report and, inclusive dates)

Master's Thesis; June 1973

5. AUTHOR(S) (First name, middle initial, last name)

Kenneth Scott Bates, Jr.

6. REPORT DATE	7a. TOTAL NO. OF PAGES	7b. NO. OF REFS
June 1973	54	8

8a. CONTRACT OR GRANT NO.	9a. ORIGINATOR'S REPORT NUMBER(S)
b. PROJECT NO.	
c.	9b. OTHER REPORT NO(S) (Any other numbers that may be assigned this report)
d.	

10. DISTRIBUTION STATEMENT

Approved for public release; distribution unlimited.

11. SUPPLEMENTARY NOTES	12. SPONSORING MILITARY ACTIVITY
	Naval Postgraduate School Monterey, California 93940

13. ABSTRACT

Hydraulic ram is the physical production of pressure wave wall loadings due to projectile penetration and their effect on a fuel cell. Facilities were designed and testing conducted in preparation for investigation of the hydraulic ram phenomenon. A ballistic range was designed that yielded projectile velocity and flight attitude information before and after wall penotration. Wall specimens of a single thickness were impacted by a range of projectile sizes, weights, shapes, and velocities. This yielded the energy absorbed by the wall without fluid damping.

DD FORM 1 NOV 68 1473 (PAGE 1)

S/N 0101-807-6811

UNCLASSIFIED

Security Classification

A-31408

14. KEY WORDS	LINK A		LINK B		LINK C	
	ROLE	WT	ROLE	WT	ROLE	WT
Hydraulic Ram						
Ballistic Range						
Projectile						
Penetration						
Survivability						

Aircraft Fuel Tank Entry Wall-Projectile Interaction Studies

by

Kenneth Scott Bates, Jr.
Lieutenant, United States Navy
B.S., United States Naval Postgraduate School, 1972

Submitted in partial fulfillment of the
requirements for the degree of

MASTER OF SCIENCE IN AERONAUTICAL ENGINEERING

from the

NAVAL POSTGRADUATE SCHOOL
June 1973

Author 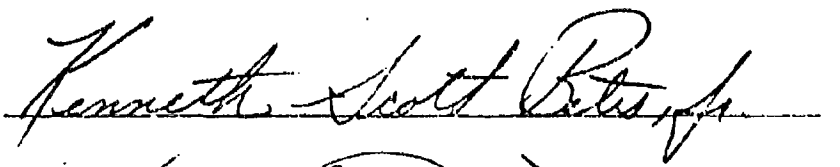

Approved by: 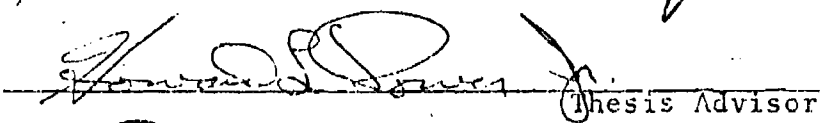
Thesis Advisor

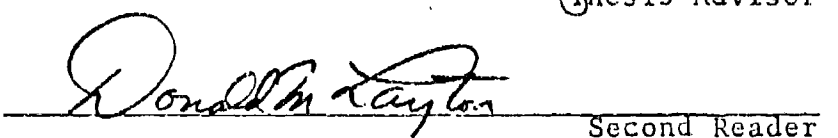
Second Reader

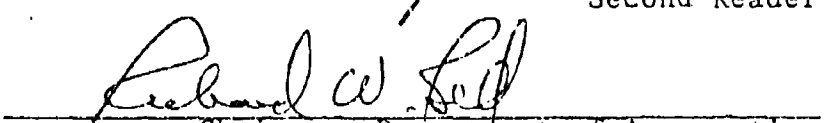
Chairman, Department of Aeronautics

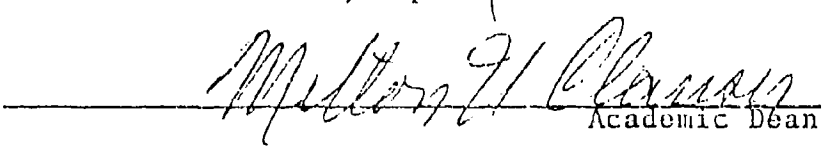
Academic Dean

ABSTRACT

Hydraulic ram is the physical production of pressure wave wall loadings due to projectile penetration and their effect on a fuel cell. Facilities were designed and testing conducted in preparation for investigation of the hydraulic ram phenomenon. A ballistic range was designed that yielded projectile velocity and flight attitude information before and after wall penetration. Wall specimens of a single thickness were impacted by a range of projectile sizes, weights, shapes, and velocities. This yielded the energy absorbed by the wall without fluid damping.

TABLE OF CONTENTS

LIST OF FIGURES

ACKNOWLEDGEMENTS

The author would like to express his appreciation to those persons who contributed to the success of this research. A particular vote of thanks is extended to Bob Smith, Electrical Engineering Research and Development Technician, who designed the ballistic range delay circuitry. Great appreciation is also extended to Bob Besel, Ted Dunton, and the rest of the staff of the Aeronautics Department Technicians for their invaluable assistance. The author would also like to thank his thesis advisor for the patience he exhibited throughout the development of this research.

I. INTRODUCTION

Aircraft survivability has been a problem of interest since the days the Red Baron shot Spads and SE-5's out of the sky in World War I. The advances in technology since these early days of aviation have made present-day aircraft very complex, sophisticated weapons systems. Today's aircraft have unsurpassed performance in the flight regimes for which they are designed. However, notwithstanding the tremendously advanced state of the art, aircraft survivability remains a serious problem of a complex nature.

The increase of interest in aircraft survivability has been directly stimulated by the tremendous rise in cost per copy of today's aircraft, as compared with those of as recent vintage as were used in Korea. The several million dollar price tag on today's weapon system brings much attention to aircraft losses. The air war in Vietnam has accounted for many of the losses in recent years. The various threat environments in Vietnam ranged from small arms fire to surface-to-air missiles (SAM's). Projectile impact or impact by warhead fragments is the major factor in generating catastrophic failure of aircraft components. If these projectiles or fragments impact into an aircraft fuel cell, the aircraft can be lost to any of several modes of damage. The kill could result from fuel starvation, fire, or explosion. The impact of projectiles into fuel cells generates intense

pressure waves in the tank fluid. The physical production of pressure wave wall loadings and their effect on the fuel cell and its components is called hydraulic ram. Hydraulic ram can be responsible for catastrophic failure of the fuel cell walls or less severe damage to the cell that would lead to one of the previously mentioned kill modes. Additionally, the hydraulic ram phenomenon could also generate damage to and failure of critical components situated outside of the cell. The study of the hydraulic ram effect is then essential to a thorough investigation of aircraft survivability.

Airframe manufacturers, as well as the armed forces, have studied the hydraulic ram effect for many years. For various reasons there has been insufficient research conducted to totally understand the phenomenon. The hydraulic ram effect can be conveniently studied by separating the event into two phases or elements; the shock phase and the cavity phase [Ref. 1]. The shock phase is generated when the projectile first enters the fluid, while the cavity phase occurs during subsequent projectile motion through the fluid. Shock wave formation due to projectile penetration into the fluid causes very high local pressures that are sometimes sufficient to cause catastrophic failure of the entry wall in the neighborhood of the entry point. Projectile penetration also produces a stress riser from which cracks propagate radially from the entry hole. For very small projectiles at high velocity (> 4000 fps) it has been shown [Refs. 2 and 3] that nearly all of the

initial kinetic energy is lost at wall impact and subsequent shock wave formation. Conversely, larger projectiles experience the greatest kinetic energy loss during fluid transit. This is also true of small projectiles at lower velocities.

As the projectile moves through the fluid it feels resistance to its motion in the form of pressure drag and viscous drag. Pressure drag is the predominant force at high velocities, generating a pressure gradient between the projectile surface and the fluid. This causes the surrounding fluid to move away from the surface of the projectile. This fluid motion accelerates the fluid to the point where its momentum is great enough to break the fluid away from the projectile's surface. When the fluid breaks away it leaves a void, commonly called a cavity. The cavity is, therefore, formed by fluid flow separation [Ref. 4].

The projectile's kinetic energy transfer to the fluid during cavity formation is due to the pressure drag and the resulting cavity. Cavity growth is defeated by fluid hydrostatic pressures. These pressures cause the cavity to collapse. The collapse is not total, due to the presence of fluid vapors as well as trapped air which entered during wall penetration. The cavity grows and collapses, generating pressure pulses which are long in duration and lower in amplitude than those in the shock phase, until equilibrium is reached in the fluid.

Projectile tumbling is a common occurrence. Any tumbling generates cavities of much larger area than those of stable projectiles. The tumbling increases the pressure drag on the projectile, thereby increasing significantly the energy loss to the fluid. The resulting large cavity area generates more severe growth and collapse oscillations, which produce large pressure pulses and more intense tank structural loadings.

The major factor that determines the severity of hydraulic ram is the manner and rate of energy transferred to the tank from the projectile. It is this release of energy in various modes that creates the total hydraulic ram effect. Other significant variables are the amount of ullage, tank material, tank structural configuration, and type of fuel. However, the amount of energy release remains the single most important variable. It is for this reason that in order to study hydraulic ram, an accurate means of measuring projectile kinetic energy is essential.

A ballistic range to be used for investigations of the hydraulic ram effect was designed with several salient features in mind. Of paramount important was a consistently accurate method for determining a time history of projectile velocity. Since projectile attitude was also of interest, shadowgraph stations were required along the flight path to give a reasonable estimate of projectile attitude at impact. The electronics associated with the ballistic range should give stable, repeatable measurements and be capable of

measuring very small time intervals accurately. The ballistic range has proven to be consistently accurate for determining projectile velocity and attitude. Having a reliable means of obtaining projectile energy is the first step in any productive study of the hydraulic ram effect, and the present ballistic range design accomplishes this goal.

II. BACKGROUND

The shock phase of the hydraulic ram effect can be separated into several events. A description of each of these in their order of occurrence is presented in this section. Dynamic stresses are generated in a fuel tank wall when impacted by a projectile. These stresses are due to the cratering and puncturing action on the wall from the projectile impact. The cratering action generates radial compressive stresses and circumferential tensile stresses in the wall. Following wall penetration the elastic strain energy absorbed during cratering is released, inducing radial tensile and circumferential compressive stresses [ref. 3]. Since the wall resists shearing, dynamic flexural stresses are generated by the puncturing action. Once the projectile has penetrated the tank wall, the impact on the fuel by the projectile generates a pressure wave emanating from the impact point. Additional tank wall stresses are induced by the pressure wave which may be large enough, when added to those produced by cratering and puncturing, to cause catastrophic entry wall fracture. The stress concentration produced by projectile penetration considerably reduces the wall stress required to induce wall failure. It has been shown [Ref. 3] that the shock phase pressure pulse is a major destructive factor for small, high-velocity (> 4000 fps) projectile penetrations. These projectiles lose most of their kinetic energy at impact.

The impulsive acceleration of the fluid by the projectile during impact and penetration generates an intense pressure field bounded by a shock wave. The shock wave is approximately hemispherical in shape and propagates radially from the projectile entry point at a velocity greater than the speed of sound in the fluid. Pressure field intensity is directly dependent upon the amount of energy transferred to the fluid by the projectile. The transferred energy is dependent upon the initial kinetic energy of the projectile as well as on its geometric shape, fluid properties, fuel tank wall construction, and wall material [Ref. 2]. The main parameters controlling shock wave strength are the energy transferred to the fluid at projectile impact and the fluid's equation of state. References 2, 3 and 6 study this formation of a hemispherical shock wave produced at projectile penetration. The shock wave's position varies with time approximately to the 0.8 power during the initial stages of expansion, and the wave becomes acoustic during the latter stages of motion. Reference 2 indicates that the initial kinetic energy of the projectile is the major parameter that determines shock wave motion. Even though the peak pressure of the shock phase is high, the pressure field is attenuated rapidly by the geometric expansion of the shock wave. The pressure loading additionally causes the fuel tank wall to move outward, creating a rarefaction wave. This rarefaction wave contributes to shock wave weakening [Ref. 4]. The average duration of the shock phase is less than 100

microseconds. After 20 microseconds, pressures are an order of magnitude less than those existing at impact. Reference 1 has substantiated this analysis experimentally, and concludes that the shock phase produces no damage to the tank except in the immediate area of projectile penetration.

The parameters that affect the stresses induced in a fuel tank wall of a specified material and thickness can be listed in several categories. The first set of parameters deals with the dynamic stresses in the wall due to projectile impact and penetration. These stresses are functions of projectile velocity, material or density, size, and projectile shape. The second set are due to fluid pressures and are functions of fluid density, fluid static pressure, fluid sonic velocity, fluid temperature, and all of the previously mentioned projectile characteristics.

A third category of parameters involves tank wall material variances. The wall fracture strength would be dependent on the amount of cold working and heat treatment. The shape and size of the entry hole, as well as cracks produced at impact, are pertinent to wall fracture strength. Finally, material strength properties at high-strain-rate loading, and at the fluid temperature, are basic variables affecting the fracture of a tank wall. In some cases the shock phase itself may not be sufficient to cause tank wall failure, but it can weaken the structure to a point where significantly less pressure is required for wall fracture in the latter stages of hydraulic ram. The shock phase is

a distinct part of hydraulic ram, and is analytically extremely difficult to model. Regardless of its overall significance to catastrophic tank failure, it can be detected and studied experimentally with relative ease.

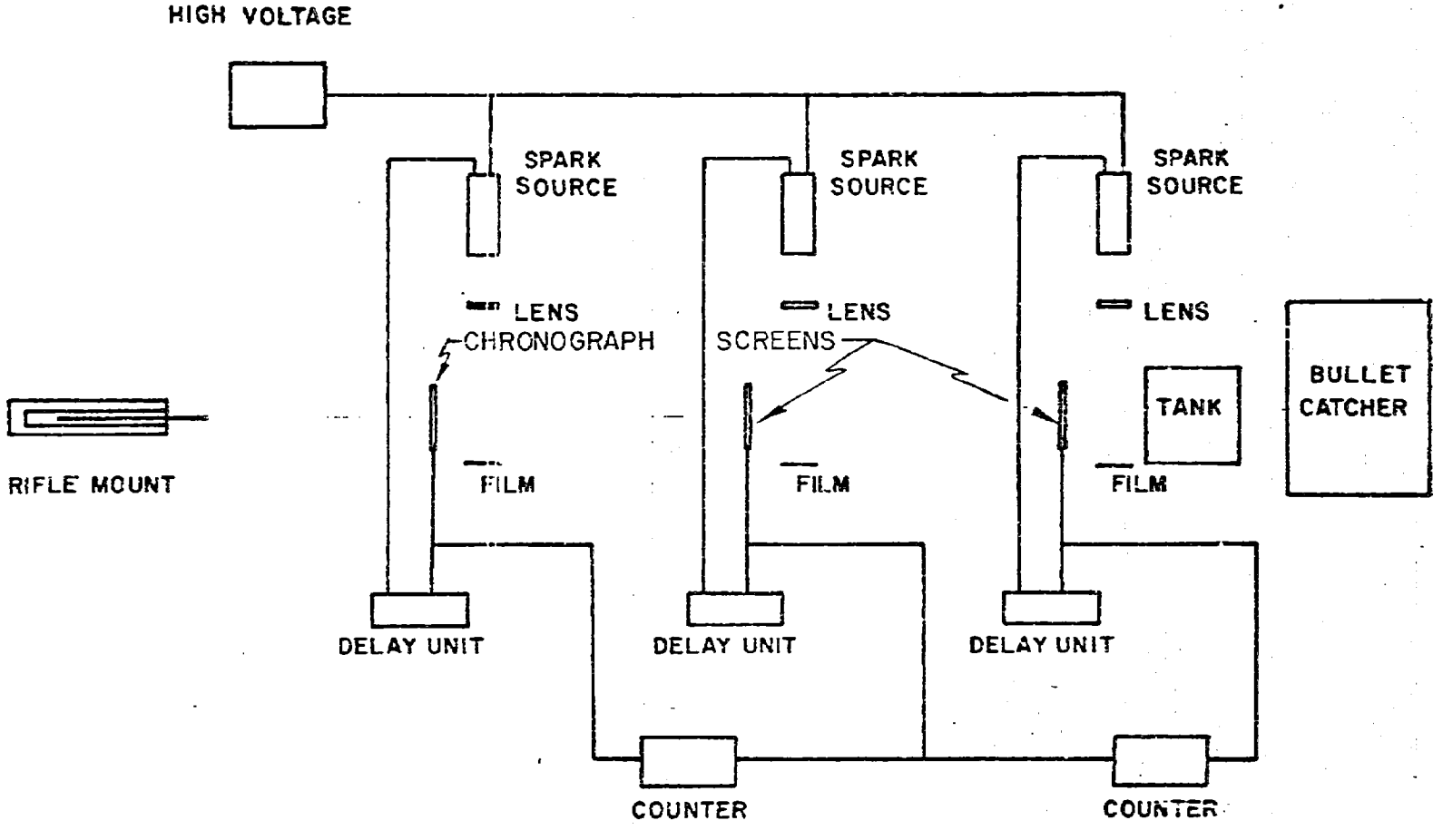

FIGURE 1
BALLISTIC RANGE COMPONENTS

III. DESCRIPTION OF BALLISTIC RANGE COMPONENTS

Basic elements of the ballistic range are shown in Figure 1. The rifle mounting system is composed of the rifle mount and the rifle mount stand. The rifle mount was made adjustable in azimuth (±8 degrees) and elevation (+3 degrees, -5 degrees) for ease in boresighting. Rifles of 22.2 and 30 caliber were held in position by the rifle mount. The rifle mount stand was constructed primarily of quarter-inch steel channel. The massiveness of the stand provides the necessary mount stability, while mount leveling is achieved by large steel bolts located in the legs of the stand. Figure 2 shows the complete rifle mounting system, and Figure 3 shows the rifle mount in detail.

The shadowgraph stations are composed of a bullet sensor, time delay unit, spark source, collimating lens, and a shadow box with reference grid for mounting the Polaroid film holder. Figure 4 shows the typical shadowgraph station setup. The bullet sensor is a chronograph screen that has a five-volt d.c. signal shorted to ground across it. When the screen is broken by a bullet, the signal is sent to the delay unit input and to a counter. Two counters are used for velocity measurement. The first sensor starts the first counter. The second sensor stops the first counter and starts the second one, and the third sensor stops the second counter. In this manner, the average velocity between

sensors is obtained which allows a prediction of the impact velocity at the tank entry wall. Monsanto 101B counters are used. They are 1 MHz counters that have a time-base accuracy of ±7 parts in 10^6 for ±10% line voltage variation. The mode in which the counters are used has an accuracy of ±1 count ± time base accuracy ± the two trigger errors. Trigger errors are less than ±0.3% of one period for sine waves with signal-to-noise ratios of 40 db or better. The delay units generate time delayed pulses ranging from 190 μs to 1700 μs. Figure 5 shows the circuitry of the delay units. A spark source triggering capacitor is built into the delay unit. This capacitor is discharged after the proper delay and causes the spark source to fire. The light from the spark is collimated by a lens. The grid on the shadow box may be used to measure the position of the bullet from the sensor as well as its attitude. Figures 6 and 7 show typical shadowgraphs taken along the bullets' trajectory. The complete shadowgraph station was mounted on a six-inch I beam which was in turn mounted on an eight-inch support beam aligned with the bullet flight path as shown in Figures 8 and 9.

The bullet catcher is shown in place in Figure 10. The top, bottom, and sides of the catcher were made from 1/2-inch aluminium, with two plates of 3/8-inch steel for the backstop. The front of the catcher was three feet square and had three 3/8-inch plywood baffles inserted into this area. The steel plates were mounted at an angle of 45

degrees to the flight path of the bullet. This was to insure deflection of the bullet downward into a layer of sand below the backstop. In this manner, the probability of ricochets from the catcher was insignificant. The baffles retard any small fragmentary ricochets. The catcher was mounted on a table-like stand constructed of wood, as shown in Figure 10.

Figure 11 shows the test apparatus used for the initial test phase. A test plate mounting frame was bolted to the support stand, on which a test plate clamping bracket was fastened. The test plates were clamped in place for testing in this manner. As seen in Figure 11, two bullet sensors are mounted directly behind the test plates. The sensors are two feet apart with the first sensor located six inches behind the test plate. These sensors have a large frontal area and use make circuits to insure accurate timing since bullet direction may change unpredictably after test plate penetration. The sensors consist of two sheets of aluminium foil separated by a thin sheet of paper which keeps the circuit open until the projectile completes it. The trigger circuit is simply a potential across the two foil sheets which is shorted when the projectile is in contact with both sheets. The first sensor starts a counter while the second one stops it. The average velocity after plate penetration is measured in this manner. Figure 12 is a shadowgraph showing a typical projectile after plate penetration. The spallation generated by plate penetration is clearly evident in this shadowgraph.

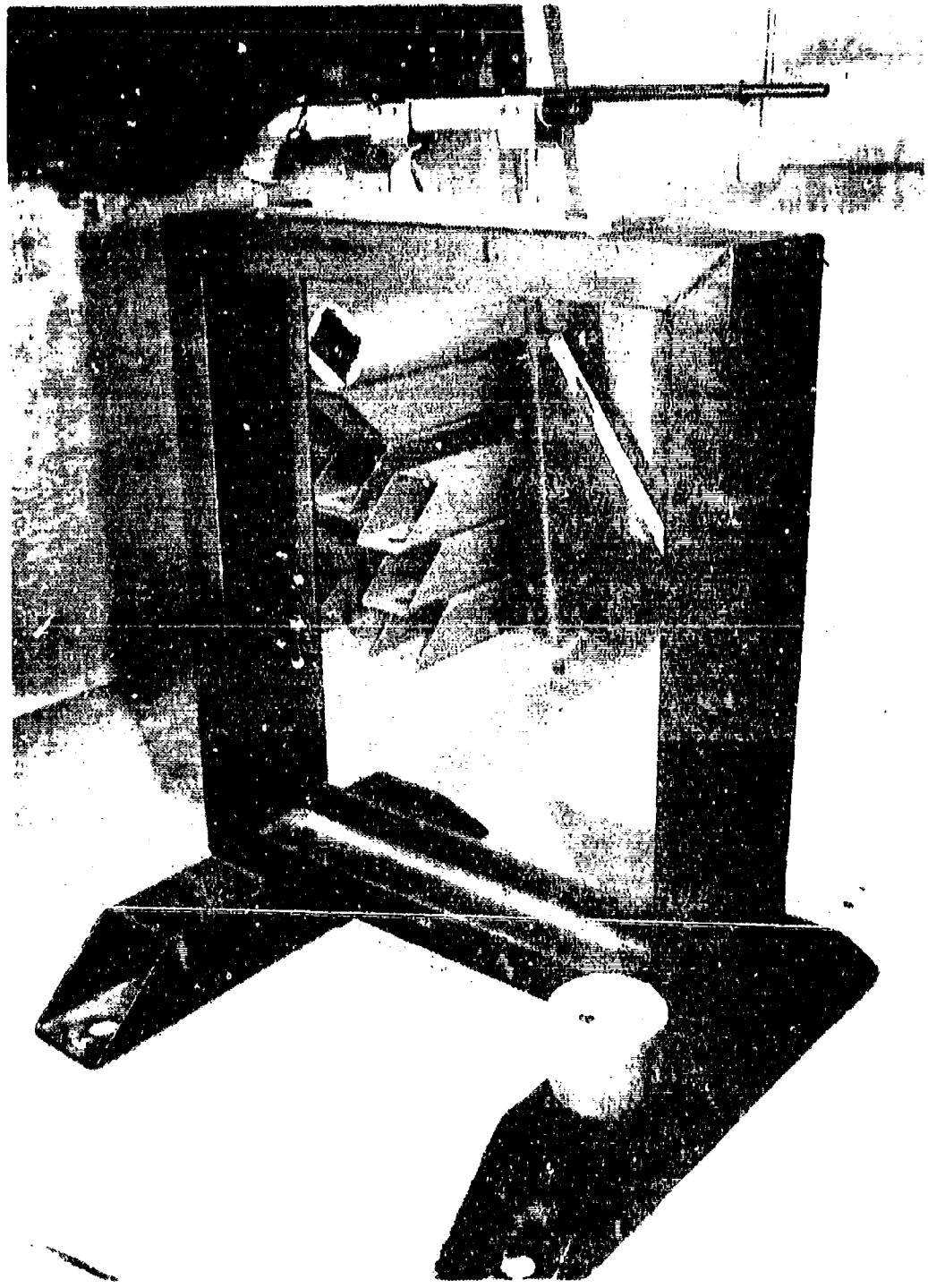

Figure [illegible] Range Rifle [illegible]

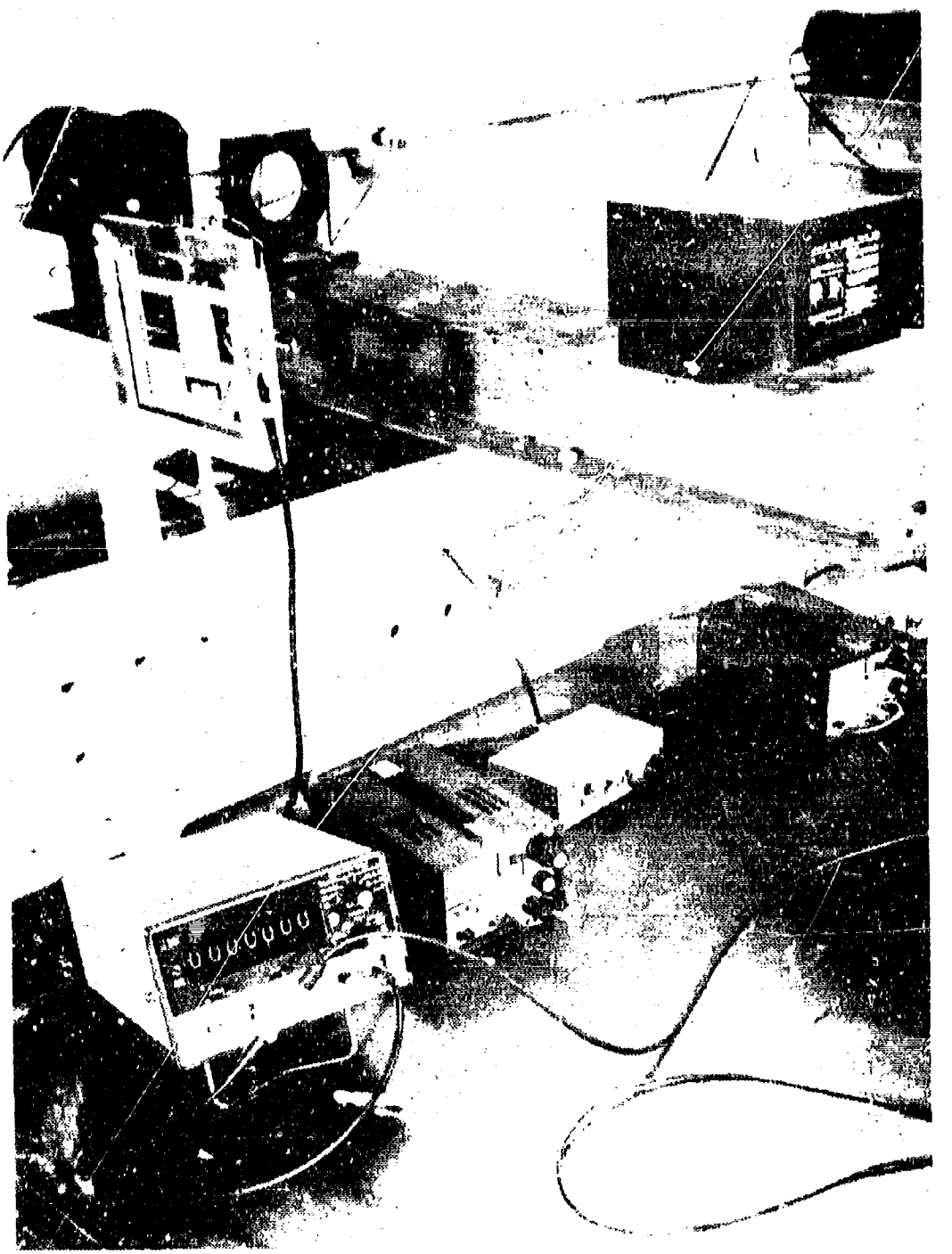

Figure 4. Ballistic Range Shadowgraph Station.

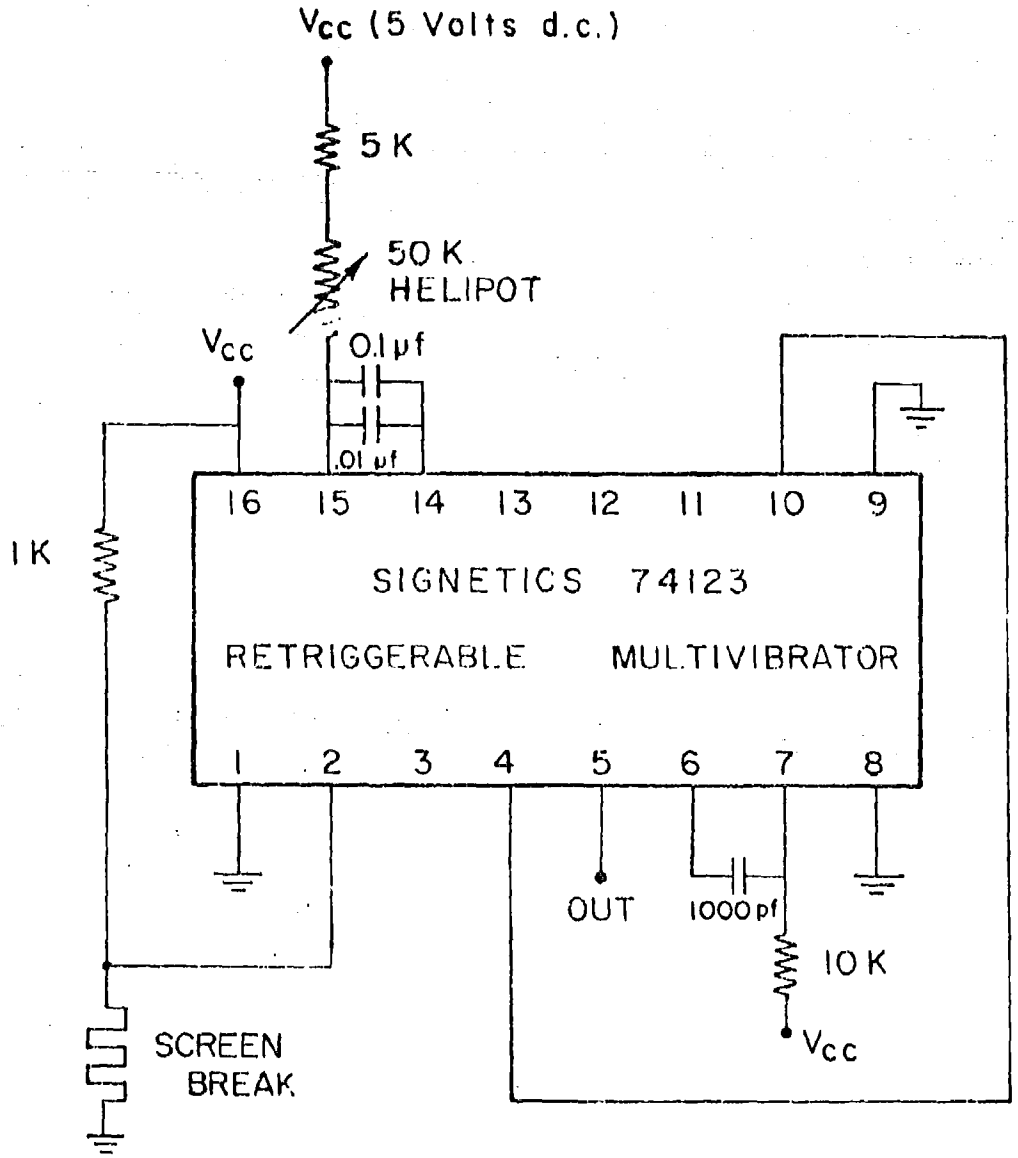

FIGURE 5 DELAYED PULSE GENERATOR CIRCUITRY (VARIABLE)

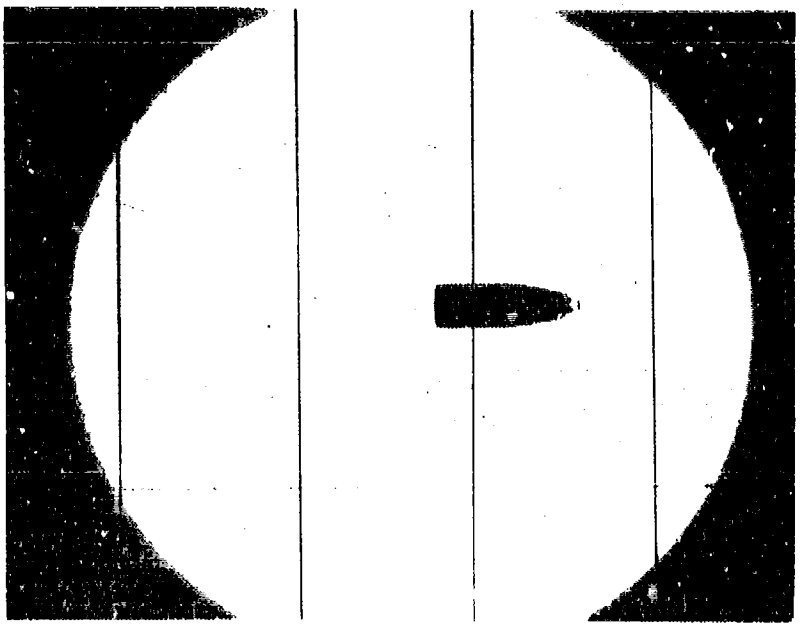

Figure 6. Shadowgraph of a 63gr Semi Point with a Velocity of 2941 fps.

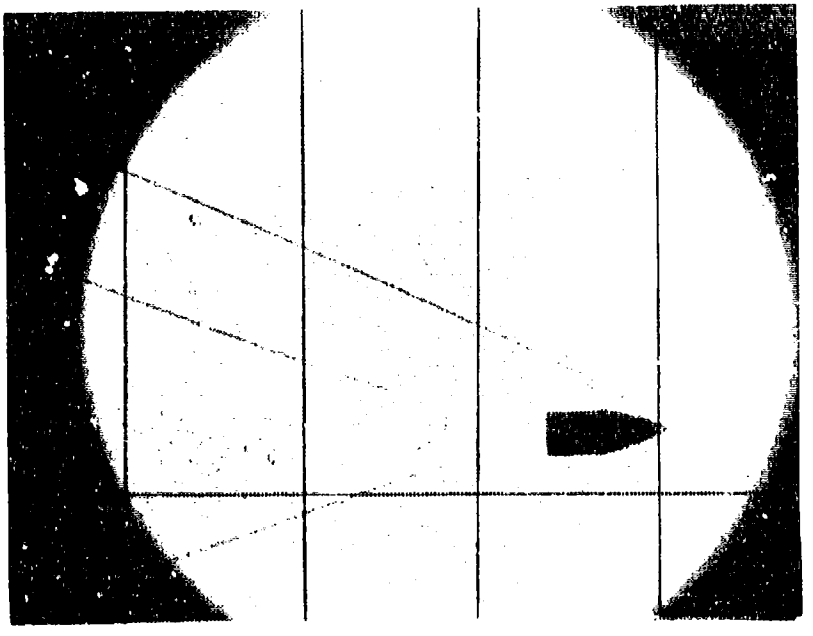

Figure 7. Shadowgraph of a 50gr Spitzer Used in Range Calibration with a Velocity of 3080 fps.

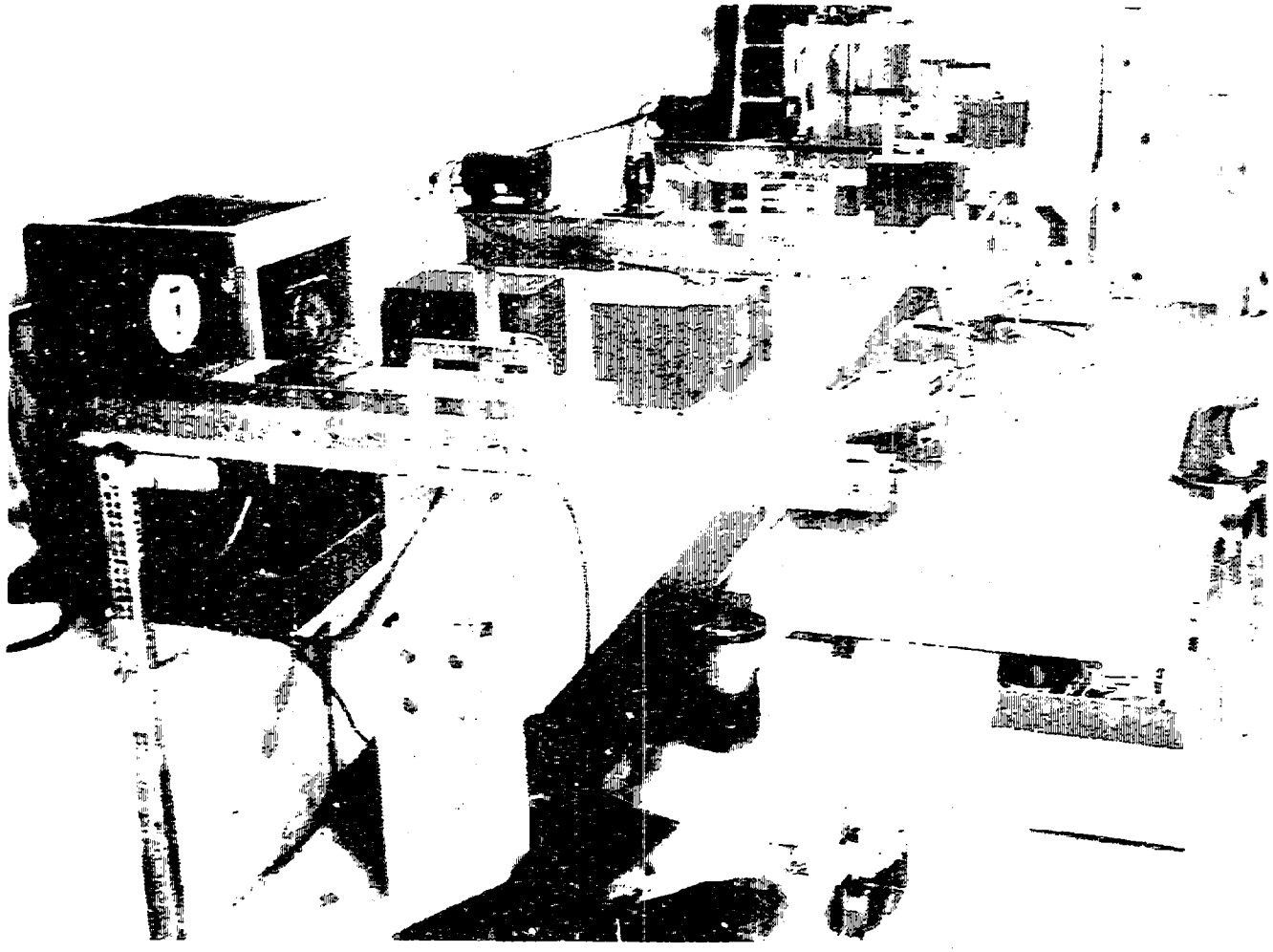

Figure 5. Ballistic Range Configuration (Test Range View).

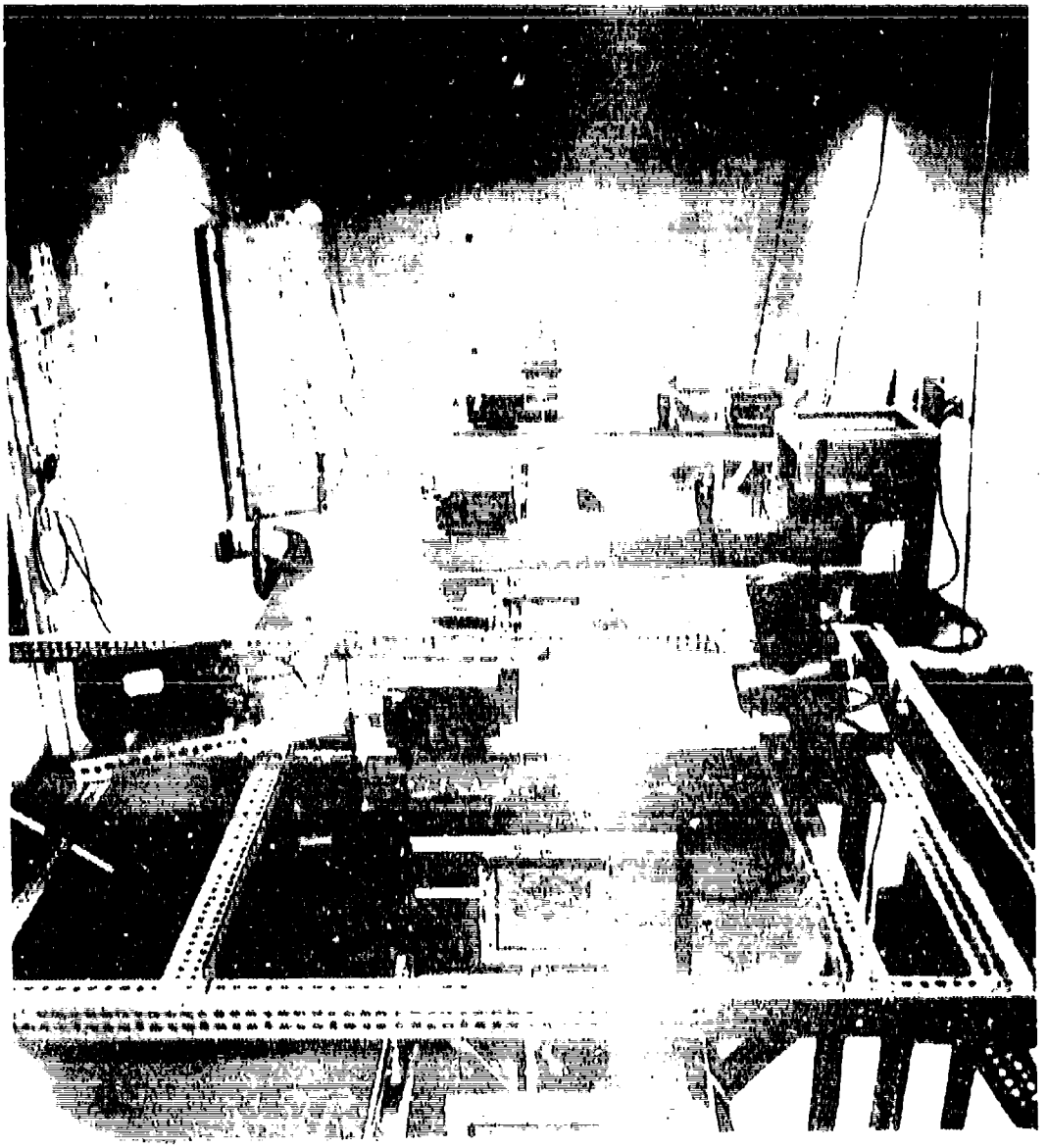

Figure 9. [illegible]

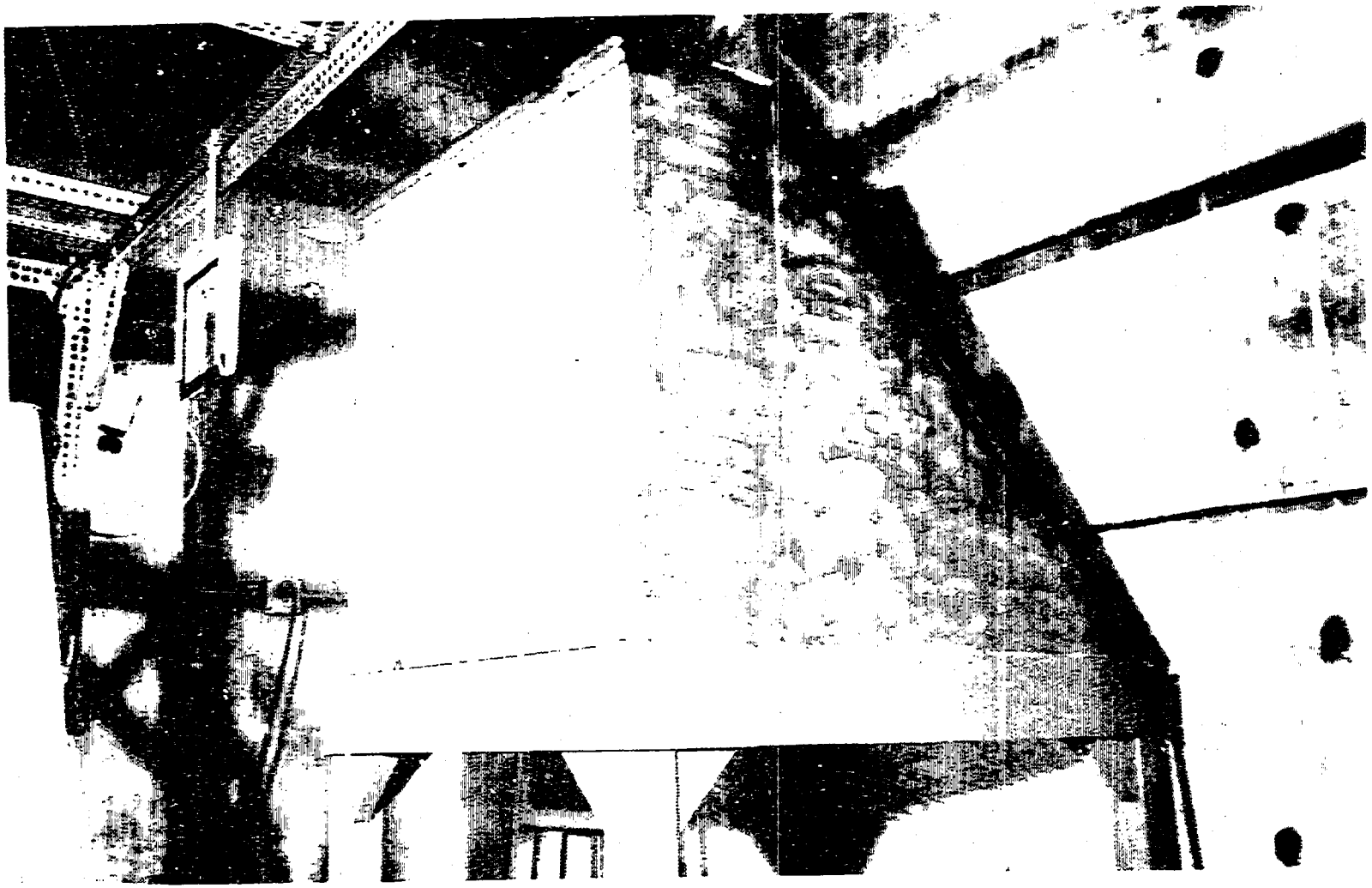

Figure 10. Ballistic Range Bullet Catcher.

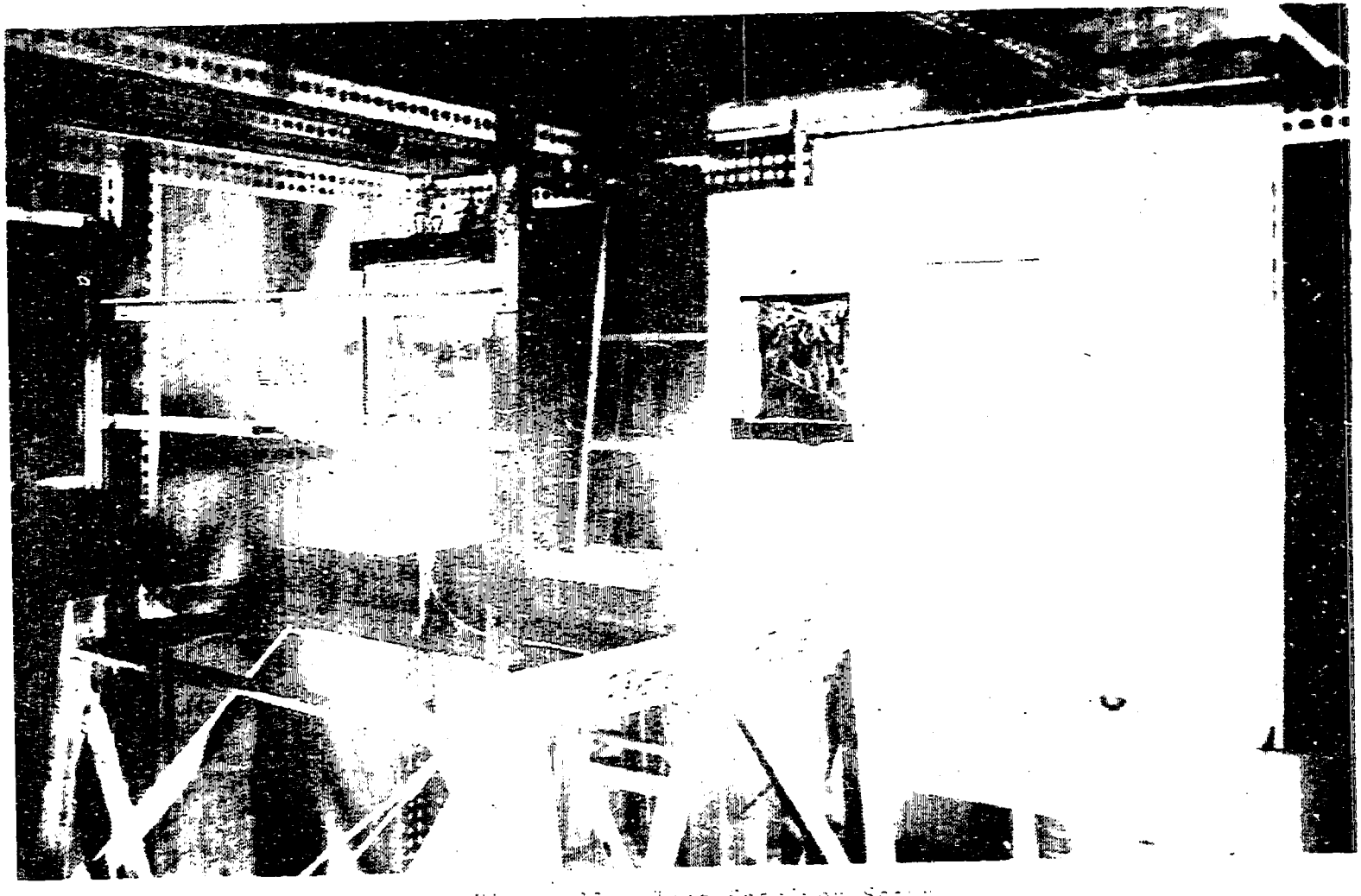

Figure 11. Test Specimen Setup.

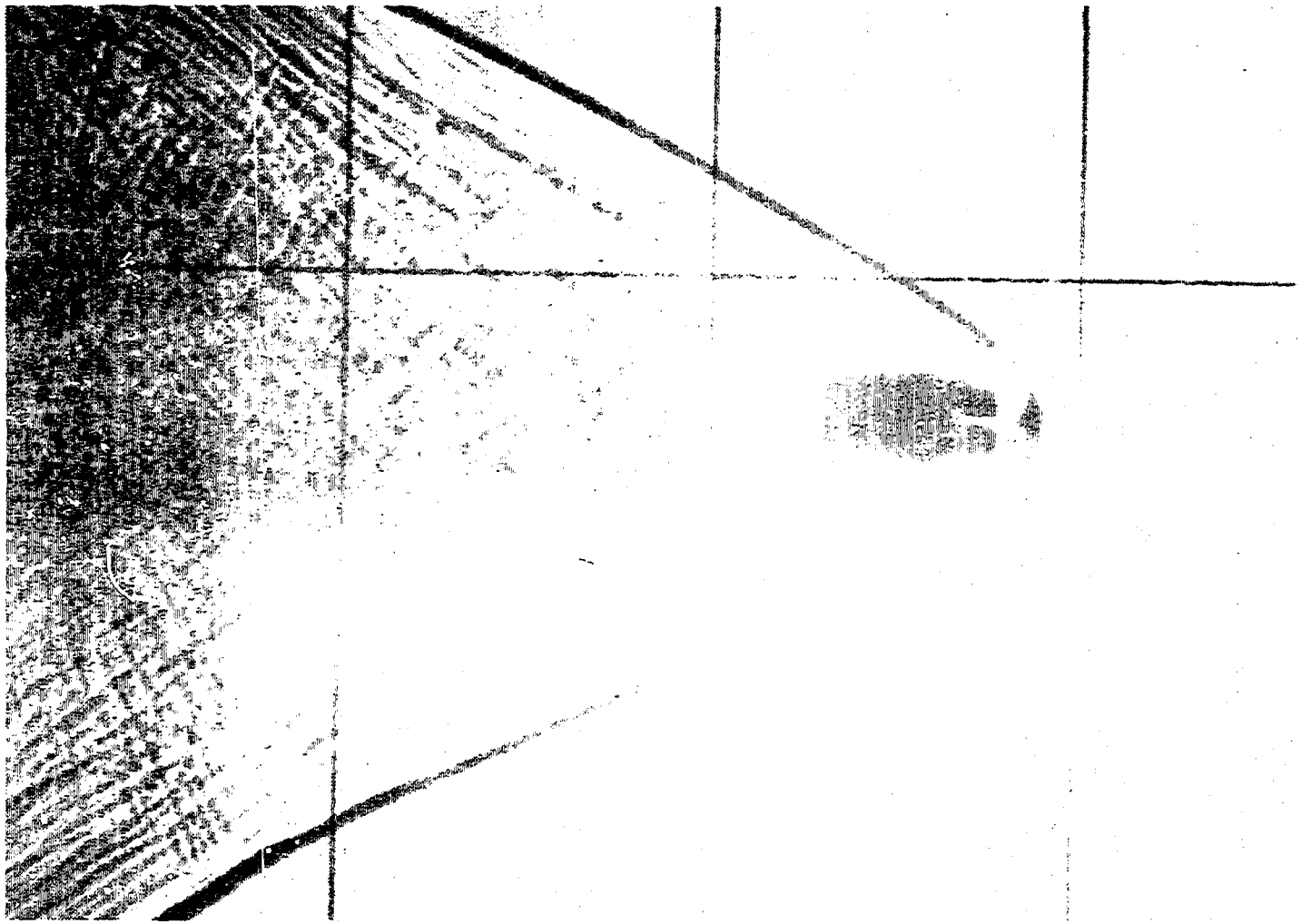

Figure 12. Flow Field after Plate Penetration.

IV. TESTING PROCEDURE

Initial testing was conducted to gain some useful knowledge of aircraft fuel tank-projectile penetration characteristics during hydraulic ram. Metal plates of 7075-T6 aluminium 0.090 inches in thickness were used in the first phase of testing. Projectiles of three masses and shapes were fired into these plates from a .222 Remington rifle. The cartridges were hand loaded to achieve a range of velocities for each projectile. The projectile velocity was measured before and after plate penetration. Several shots at each mass, shape and velocity were fired to provide statistical data. This phase of testing was conducted in order to determine the energy lost by the projectile during penetration of entry wall material alone. A second purpose was to determine the sensitivity of penetration energy loss to projectile shape, weight, and impact velocity.

Future phases of testing will consist of shooting into a fluid-filled test tank through pre-drilled holes in the entry wall. The same spread of projectile shapes, weights, and velocities will be used. The velocity before impact will be measured, as well as the velocity decay in the fluid. The purpose of this test phase is to determine the average kinetic energy loss of the projectile without entry wall penetration, but with fluid-entry wall interaction. A second purpose is to ascertain the susceptibility to tumbling

in the fluid of the various projectile shapes. The third phase of testing will be conducted by shooting the various projectile shapes, weights, and velocities into the test tank with a solid entry wall. Projectile velocity before penetration will be measured as well as velocity decay of the projectile in the test tank. The result of this phase will be a measure of the kinetic energy loss due to entry wall penetration and projectile-fluid interaction, i.e., hydraulic ram production.

The overall intent of this testing is to determine the total amount of energy available for transfer to the fluid medium after entry wall penetration. The first phase determined the energy loss due to wall penetration without fluid damping. The second phase will yield the amount of projectile energy loss to the fluid with entry wall interaction but with no penetration losses. The third phase should give the amount of energy the projectile loses during hydraulic ram generation up to a specific time after impact. Comparison of phase two with three should yield the amount of energy loss during entry wall penetration with tank fluid support. Comparison of phase one with this result should yield the difference in energy loss due to the presence of the fluid medium. That is, the energy loss associated with entry wall-fluid interaction, during the impact and shock phase, should become deterministic.

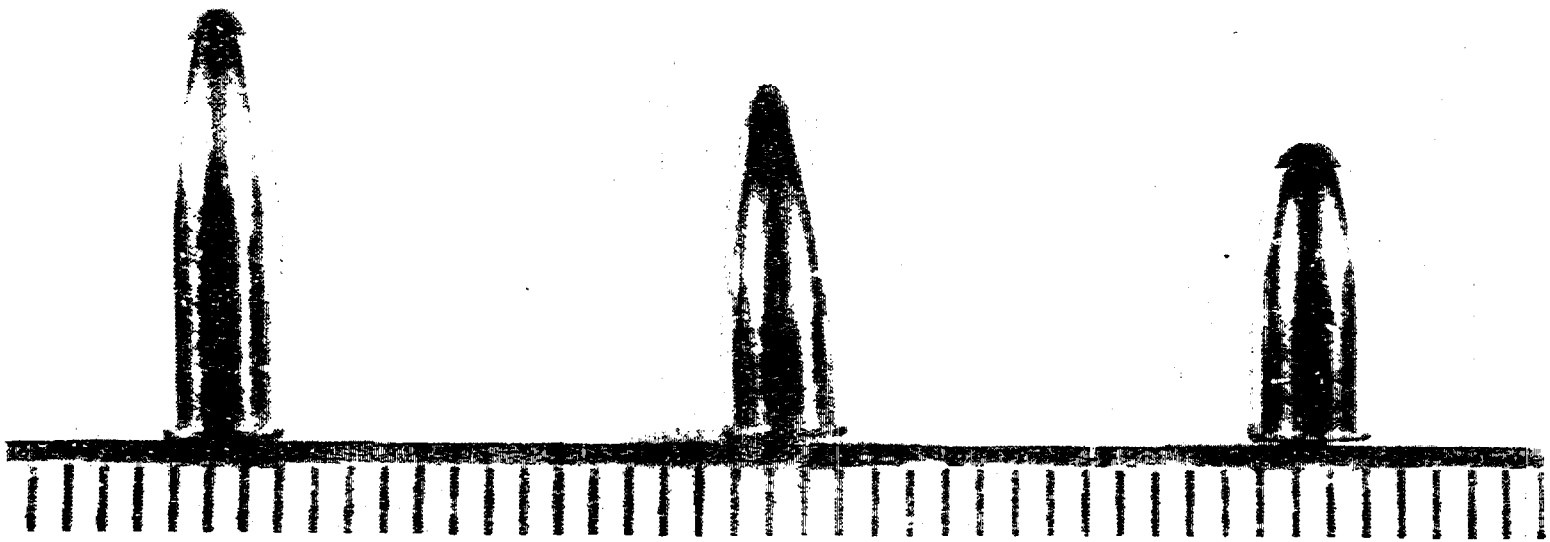

Figure 15. Shapes of Various Projectiles Used in Testing.

V. DISCUSSION OF RESULTS

Phase one testing was conducted to determine the energy loss of various projectiles during penetration of entry wall material without fluid damping. The results of those tests are presented in this section. The various shapes of the projectiles used in the tests are shown in Figure 13. Determination of shape and mass effects on material penetration velocity loss was also an endeavor of phase one testing.

Previous work by Forman, et al. [Ref. 7] derived equations for the penetration velocity (ballistic limit) and the projectile exit velocity. The equations for these projectile velocities, valid for impact velocities less than 4000 fps [Ref. 7], are:

$$V_o = \sqrt{\frac{2\pi Gr}{15m}\,(1.6\ t - 4/3)} \qquad (1)$$

and

$$V_e = V_o\sqrt{(V_i/V_o)^2 - 1} \qquad (2)$$

where V_o is the penetration velocity, V_e the exit velocity, and V_i the impact velocity. Equation (1) was derived from Dunn's solution for the penetration depth (P) of a rigid sphere into a semi-infinite deformable solid and is written as follows:

$$P = (mV_i^2)/(2\pi\sigma_{YT}r) + 1/3r \qquad (3)$$

The variable r is the radius of the hole produced in the impacted specimen, which is assumed to be the same as the radius of the projectile. Equation (3) assumes that P is proportional to material thickness, t, and that $\sigma_{YT} = G/15$, where G is the shear modulus of the target material. These two quantities are substituted into Equation (3) to yield Equation (1).

For impact velocities much greater than V_o, the projectile exit velocity, V_e, approaches the impact velocity. For this reason it was concluded [Ref. 7] that an equation relating V_i with V_e, assuming a constant kinetic energy loss, could be written in its presented form. Equation (2) yields a theoretical plot of the manner in which the exit velocity might be expected to vary as shown in Figure 14. Figure 14 also shows the experimental variation of exit velocity versus impact velocity for two 22.2 caliber projectiles of equal mass, but with different nose shapes. The K.E. loss is assumed to be independent of impact velocity. Since Equations (1) and (2) depend only on test plate material, thickness, bullet diameter and mass, the nose shape effects are not predicted in Figure 14. The data points for both shapes in Figure 14 agree closely with the theoretical prediction of Equation (2). This indicates that nose shape has a minor role in determining the exit velocity.

Typical damage to the front face of tested material plates using spitzer projectiles [Fig. 13] is shown in Figure 15. All tested plates that were penetrated by projectiles with impact velocities greater than 2200 fps showed similar damage. The exit face of these plates is shown in Figure 16. For impact velocities less than 2200 fps the test plates have a region of plastic deformation or bending in the direction of impact. The target area suffering plastic deformation decreases with increasing impact velocity [Ref. 8] and is not readily detectable in the tested plates above an impact velocity of 2200 fps. Similar views of test plates penetrated by hornet projectiles are shown in Figures 17 and 18. None of these plates exhibited any plastic deformation over the tested range of impact velocities. This may be explained by the following argument. The force that acts on the projectile during penetration is proportional to the cross sectional area of the projectile at low velocities [Ref. 8]. The fact that the hornet has a much more blunt nose shape than the spitzer indicates there is a smaller, more constant force acting on the hornet during penetration at low velocities. The spitzer, on the other hand, is much more slender and consequently its cross sectional area is effectively increasing during penetration. This indicates that there is a higher initial stress level at the point of impact for spitzer projectiles since the same amount of energy (as possessed by the hornet) is distributed

over a significantly smaller area. This analysis is reinforced by the fact that long, slender projectiles will generally penetrate deeper than a shorter one of equal mass at equal impact velocities [Ref. 8].

The final series of tests was conducted using projectiles of different masses with a semi-pointed nose shape. A projectile of this type is shown in Figure 13. Masses of 55gr and 63gr, respectively, were used in these tests, and Figures 19 and 20 show the results in the same manner as Figure 14. The 55gr projectile displayed excellent agreement with theory over the tested range of impact velocities. The deviation from theory is in the same direction as in the case of the hornet and spitzer, but not as severe. Figure 20 is a similar comparison of data for the 63gr projectile. These results also agree well with theory, but they are somewhat scattered in their deviation pattern. The greater length of the 63gr projectiles increases the effect that yaw or spin axis nutation has at plate impact. The more yaw present at impact, the greater the projected area of the projectile during penetration. Figure 21 shows a comparison of typical damage to the entry face of the test plates at low and high impact velocities. The exit faces of these test plates are shown in Figure 22. Both of these figures graphically demonstrate the effect of yaw on penetration damage. Plate damage was not as severe for the 55gr projectiles, as they exhibited no excessive yaw tendencies.

A plot of kinetic energy loss versus initial velocity for all the projectiles is given in Figure 23. The theoretical kinetic energy loss is invariant with initial velocity, and is therefore used in the figure as a reference for the experimentally determined data. The 63gr semi-point exhibited the greatest energy loss in relation to theory due primarily to its excessive yaw at impact. The energy loss associated with the high mass projectile is typically greater than that of the lower mass projectiles for equal values of initial velocity. Again this was essentially due to the acute yaw of the heavier projectile. The 55gr projectiles show closer agreement with theory over the tested range than do the other projectiles. The 45gr hornet shapes show a tendency to agree better with theory as initial velocity is increased. The 45gr spitzer shapes have no apparent pattern to their energy loss variation. All projectiles deviate from theory in a fairly consistent manner according to their individual types.

The results of phase one testing have demonstrated the ability of the ballistic range to accomplish its designed purpose accurately and reliably. The close agreement with theory shown by the data in Figures 14, 19 and 20 indicates the accuracy to which the velocities are measured. These figures also show that as projectile mass is increased, the exit velocity tends to be closer to impact velocity. The scatter present in the data for the 63gr projectiles in Figures 20 and 23 demonstrates the effect of yaw on energy

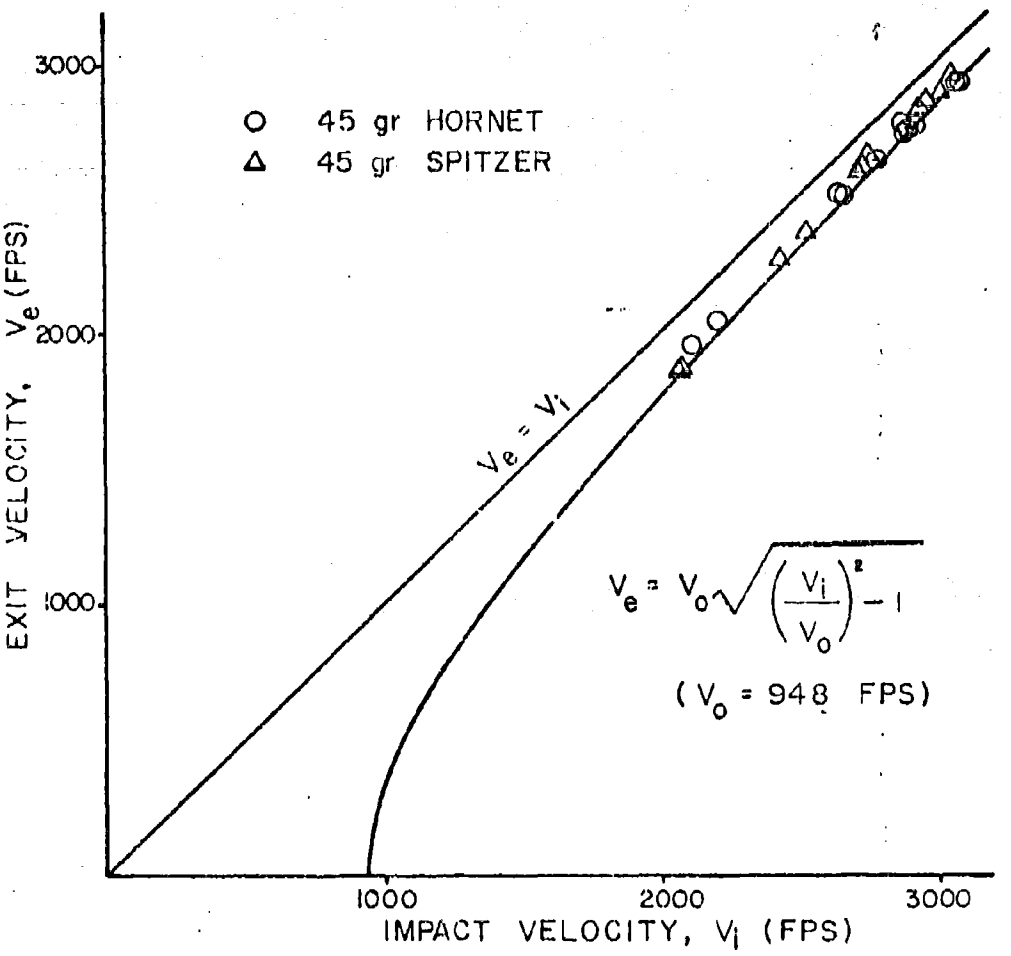

Figure 14. Exit Velocity versus Impact Velocity for Two 22.2 Caliber Projectile Shapes Fired Normal to a 0.090 inch Thick 7075-T6 Aluminium plate.

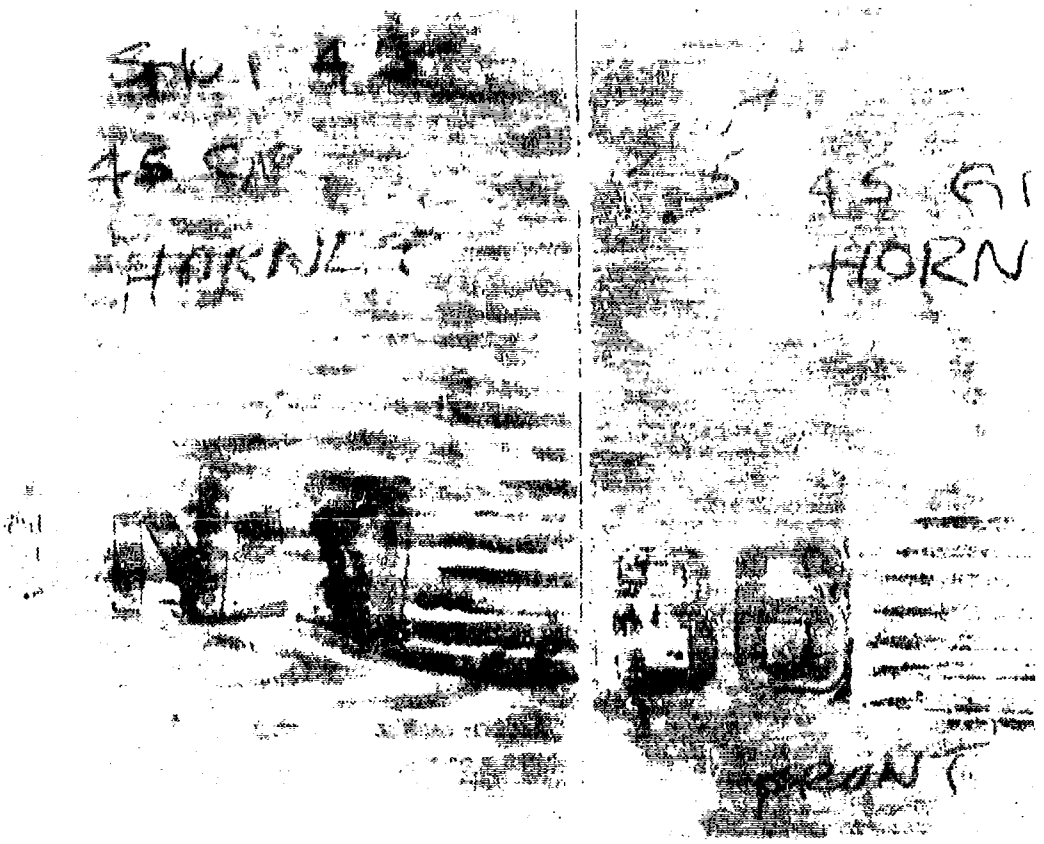

High Impact Velocity Low Impact Velocity

Figure 17. Typical Entry Damage due to 45gr Hornet Projectile Penetration.

High Impact Velocity

Low Impact Velocity

Figure 18. Typical Exit Damage due to 15gr Hornet Projectile Penetration.

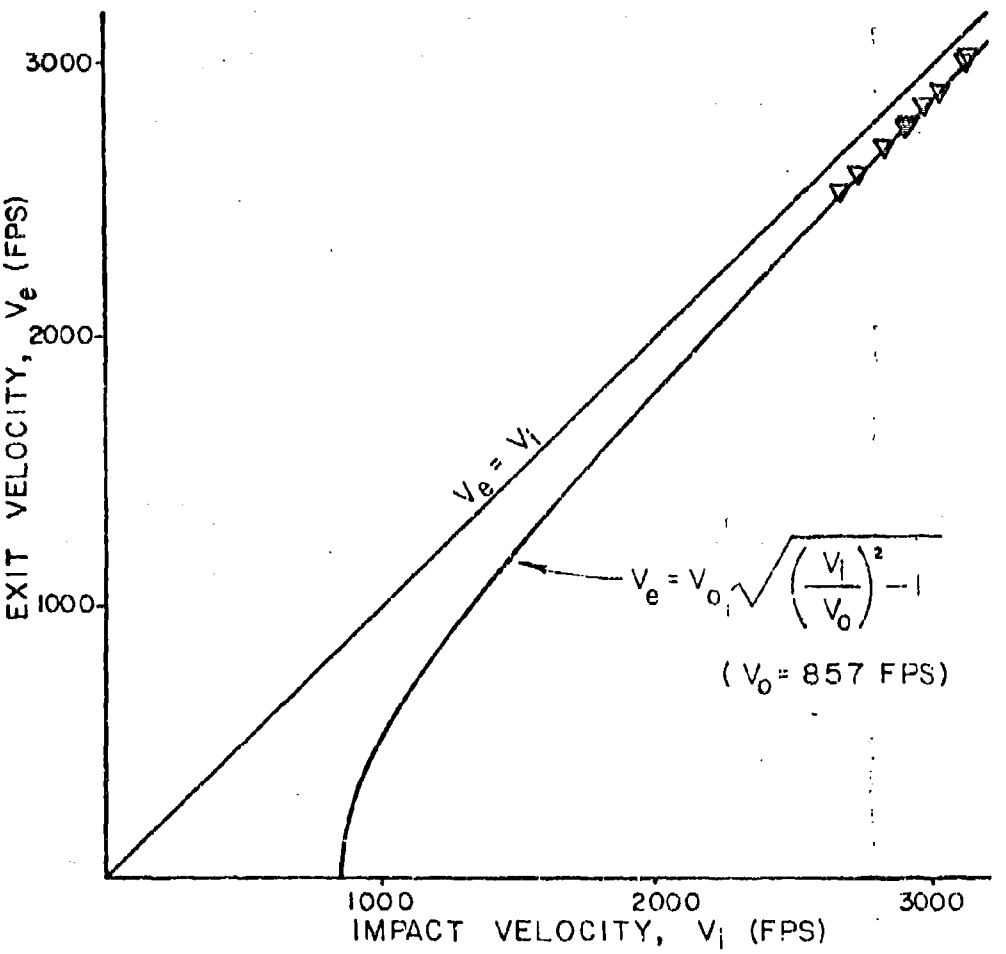

Figure 19. Exit Velocity versus Impact Velocity for a 55gr Semi-Pointed 22.2 Caliber Projectile Fired Normal to a 0.090 inch Thick 7075-T6 Aluminium Plate.

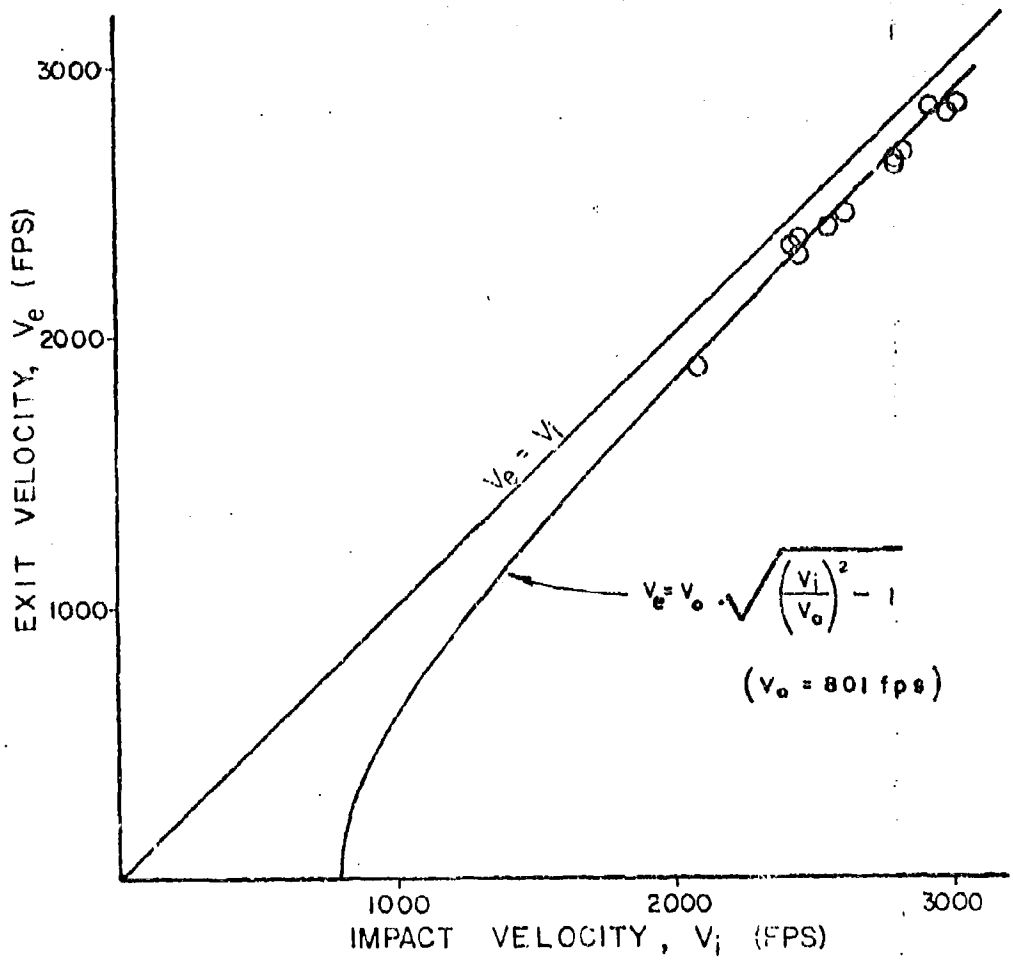

Figure 20. Exit Velocity versus Impact Velocity for a 63gr Semi-Pointed 22.2 Caliber Projectile Fired Normal to 0.090 inch Thick 7075-T6 Aluminium Plate.

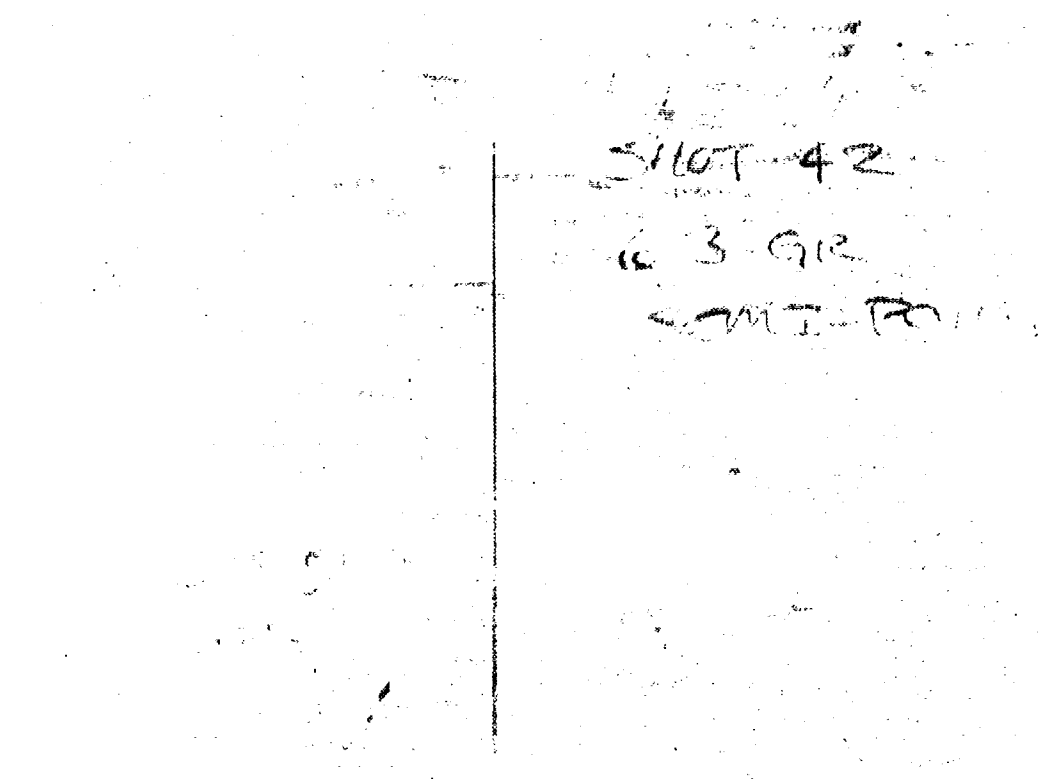

Figure 21. Typical Entry Damage due to 63gr Semi-Point Projectile Penetration.

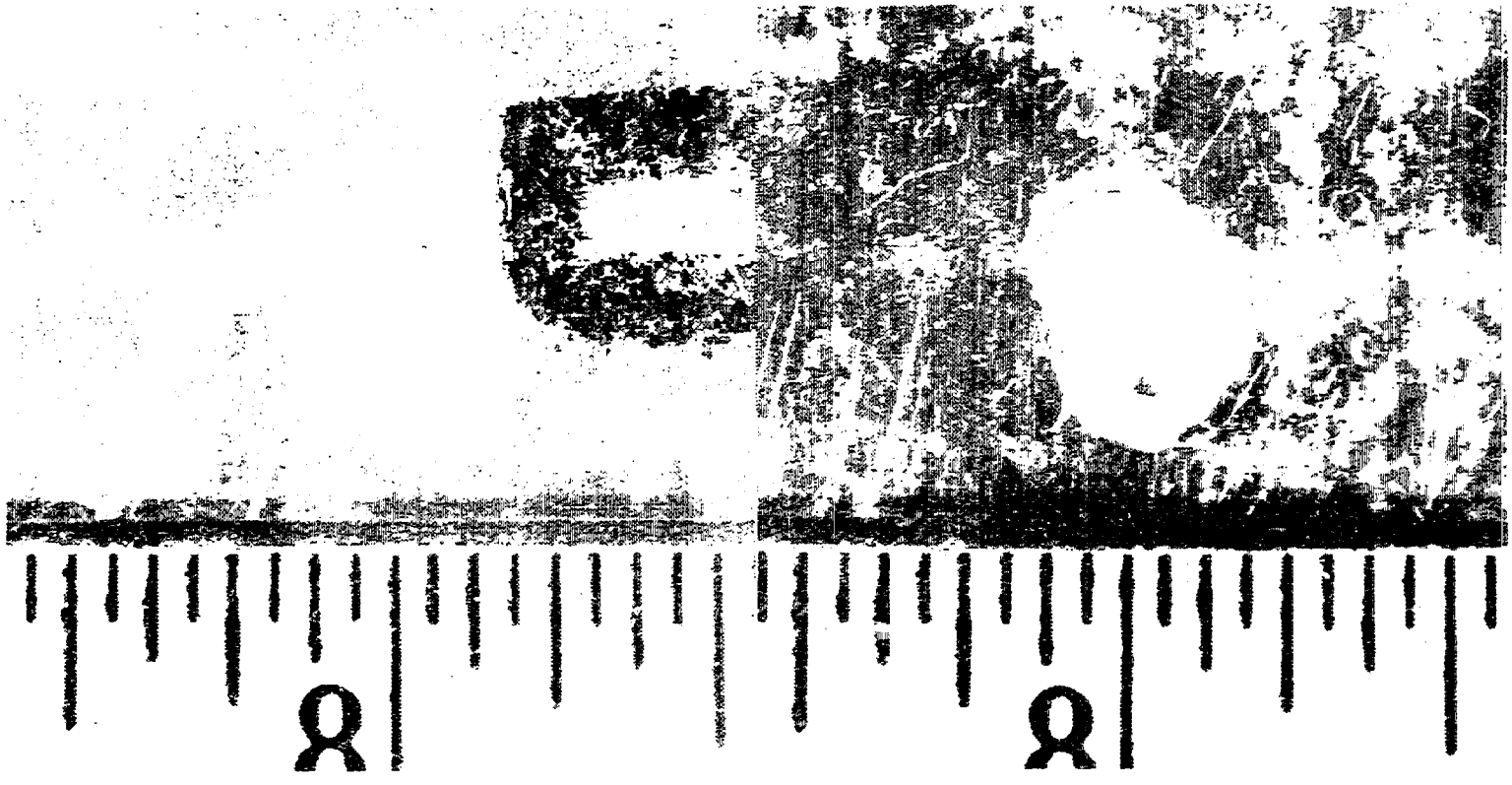

High Impact Velocity

Low Impact Velocity

Figure 22. Typical Exit Damage due to 63gr Semi-Point Projectile Penetration.

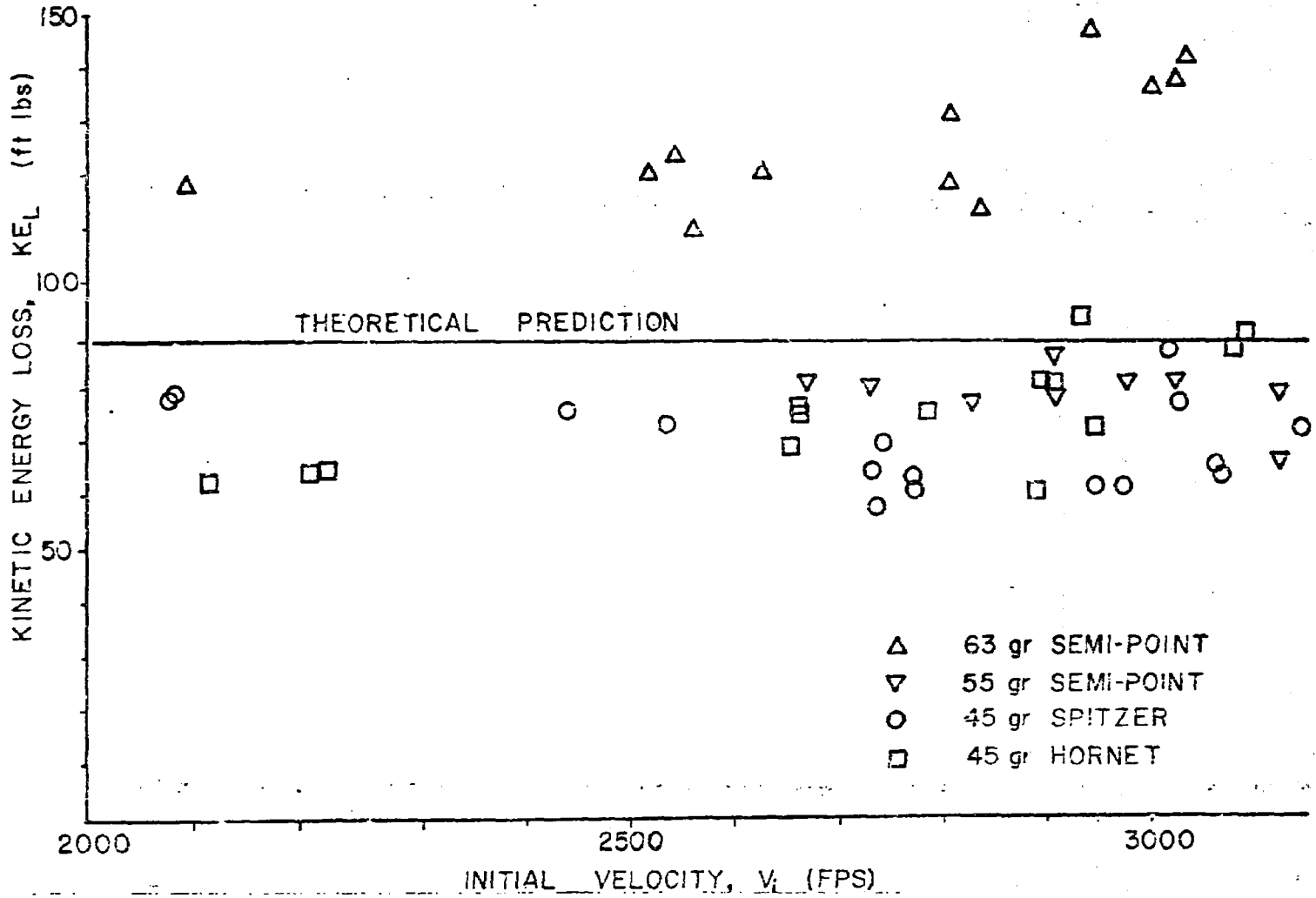

Figure 23. Plot of Kinetic Energy Loss versus Initial Velocity for a Range of Projectile Masses and Shapes.

VI. CONCLUSIONS

The first conclusion to be drawn from the completed testing is that an accurate, reliable means of determining projectile velocities has been established. The design and calibration of the ballistic range have proven to be workable and stable during phase one testing. The test results indicate excellent agreement with the theory used; however, the theory is only a first order approximation, as various higher order effects have been neglected. The results do provide a solid measure of ballistic range performance, as well as an excellent basis for studies of a second order nature. Projectile shape effects were not determinable from this phase of testing as they are essentially second order effects. In order to determine the shape effects, several entry wall material-projectile interactions must be considered and modeled. Projectile deformation due to wall impact must be considered as well as the varying strength properties of the test material under impulsive loads. Finally, the completion of phase one has been successful and has generated several well founded results, in addition to the following recommendations.

VII. RECOMMENDATIONS

The following recommendations are offered as an aid to the productive continuation of the project. In order to gain correlation of these data, the same experiments should be conducted using plates of the same material but of varying thicknesses. A greater range of velocities for the same projectiles should be used to see if the trends displayed in the current comparison plots continue. Higher velocities were not attainable with the present rifle. The use of a higher caliber projectile in the same basic tests would generate data of much higher energy levels than those obtained. These tests would broaden the scope of the hydraulic ram study effort by producing a better picture of entry wall penetration phenomena.

Finally, it is recommended that Phase II and Phase III of the outlined test procedure should be conducted.

LIST OF REFERENCES

1. McDonnel Douglas Corporation Report No. G964, Hydraulic Ram: A Fuel Tank Vulnerability Study, by R. Yurkovich, 5 September 1969.

2. NASA Technical Note D-3143, Investigation of Pressure Waves Generated in Water-Filled Tanks Impacted by High-Velocity Projectiles, by F. S. Stepka, December 1965.

3. NASA Technical Note D-1537, Preliminary Investigation of Catastrophic Fracture of Liquid-Filled Tanks Impacted by High-Velocity Particles, by F. S. Stepka, May 1963.

4. Boeing Company Report No. D162-10294-1, Hydraulic Ram, by R. G. Blaisdell, 18 September 1970.

5. Naval Weapons Center, Fluid Dynamic Analysis of Hydraulic Ram, by Eric A. Lundstrom, July 1971.

6. Physical Review Vol. 68, Nov. 1-15, 1945, Numbers 9 and 10, Shock Wave Pressures in Water Produced by Impact of Small Spheres, by J. Howard McMillen.

7. Air Force Flight Dynamics Laboratory Technical Report AFFDL-TR-67-157, Vulnerability of Aircraft Structures Exposed to Small Arms Fire Projectile Impact Damage, by R. G. Forman, W. H. Parker, A. W. Gunderson, and A. Bilek, February 1968.

8. Rinehart, J. S. and Pearson, J., Behavior of Metals under Impulsive Loads, Dover Publications, Inc., New York, 1954.